Catal Lett (2012) 142:845–853
DOI 10.1007/s10562-012-0839-8

Ni Promotion of WP/SiO_2 Catalysts for Pyridine Hydrodenitrogenation

Jan Kopyscinski · Jinsoon Choi · Lining Ding · Shihua Zhang · Blessing Ibeh · Josephine M. Hill

Received: 20 March 2012 / Accepted: 2 May 2012 / Published online: 12 May 2012

Abstract WP/SiO_2 catalysts promoted with Ni were prepared by wet impregnation with various molar ratios of Ni to W and then evaluated in the reaction of pyridine hydrodenitrogenation for pyridine conversion and product selectivity. The addition of Ni to the WP/SiO_2 catalysts resulted in increased pyridine conversion and selectivity to pentane. The molar ratios of Ni:W:P are important, because nickel and tungsten compete for phosphorous and form WP, W_3O, Ni_2P and/or W crystals.

Keywords Hydrodenitrogenation · Pyridine · $NiWP/SiO_2$ · Transition metal phosphides · XRD

1 Introduction

Due to more stringent environmental legislation, significant efforts have been made to lower the levels of nitrogen in petroleum fuels. Hydrodenitrogenation (HDN) is a process in which hydrotreating is used to reduce the nitrogen content of hydrocarbons during oil refining. Many different heteroaromatic nitrogen components including pyridines, anilines, quinolines, indoles, carbazole and their alkylated derivatives exist in petroleum feedstocks. Typically, however, pyridine is used as a model compound for studying HDN over various catalysts. Conventional HDN catalysts are Ni–Mo–S and Co–Mo–S systems. Among alternatives to the conventional sulfides for HDN are transition metal carbides, nitrides, and phosphides. Metal phosphide catalysts such as WP [1–4], Ni_2P [3, 5–8], MoP [2, 3, 5, 9, 10], CoP [2], and Rh_2P [11] have been studied in recent years for HDN [1–4, 6, 9] and also for hydrodesulphurization (HDS) [3, 5–8, 10, 11].

The base phosphide catalysts have been modified with a second metal in various combinations—NiMoP [2, 5, 12, 13], CoMoP [2, 14], $CoNi_2P$ [12, 15], NiCoP [16], TiMoP [9], FeNiP [17, 18] and NiWP [19]. Although these bimetallic phosphide catalysts had higher activities, and higher selectivity towards the desired product (e.g., pentane for HDN of pyridine) compared to single metal phosphide catalysts, most of this research work has been focused on HDS reactions. As HDS and HDN are parallel reactions in the hydrotreating process, the promoting effect on the HDN reactions has been seldomly mentioned for bimetallic metal phosphide catalysts. In one paper, Abu and Smith did report that a Ni_xMoP catalyst had lower turnover frequencies for the HDN of carbazole, but a higher selectivity to bicyclohexyl compared with the MoP catalyst [13]. One of the issues with promoting WP catalysts with Ni is that Ni may compete with W for P (i.e., Ni_2P or WP). The Ni–W–P interactions and their effect on the hydrodenitrogenation of pyridine have not been investigated. Clark et al. [1] only studied the WP single system.

In this study, WP/SiO_2 catalysts modified by the addition of Ni were synthesized and tested for the HDN of pyridine. The catalysts were prepared by adding different amounts of Ni to the WP system such that the molar ratio of total metal (Ni + W) to phosphorus was 1, with a fixed amount of tungsten (17 wt%). Surface area, pore volume, CO-uptake and X-ray diffraction profiles were measured

Electronic supplementary material The online version of this article (doi:10.1007/s10562-012-0839-8) contains supplementary material, which is available to authorized users.

J. Kopyscinski · J. Choi · L. Ding · S. Zhang · B. Ibeh · J. M. Hill (✉)
Department of Chemical and Petroleum Engineering, University of Calgary, 2500 University Drive NW, Calgary, AB T2N 1N4, Canada
e-mail: jhill@ucalgary.ca

for the different catalysts. The pyridine conversion, turnover frequency, and selectivity to the reaction products were also examined. The present study was aimed at determining if adding Ni to WP had a similar effect for the HDN of pyridine as was observed for the HDN of carbazole over NiMoP catalysts [13].

2 Experimental

2.1 Catalyst Preparation

2.1.1 Ni/SiO_2 and W/SiO_2 Catalysts

The catalysts were prepared by wet impregnation of a SiO_2 support (35–60 mesh, >99 %, Sigma-Aldrich, Oakville, ON, Canada), which was dried at 393 K for 12 h prior to use. Silica as a support was chosen to minimize the interaction between phosphorous and the support that occurs with alumina supports [6, 20]. More specifically, amorphous $AlPO_4$ can be formed during preparation of Ni_xP_y on alumina supports, which requires higher reduction temperatures compared to silica supports [6, 21, 22]. Deionized water was used in the preparation of all solutions.

SiO_2 was impregnated with an aqueous solution of nickel(II) nitrate hexahydrate ($Ni(NO_3)_2{\cdot}6H_2O$, Sigma-Aldrich, Oakville, ON, Canada) to produce a Ni/SiO_2 catalyst precursor with a target nickel loading of 6.1 wt% (in Ni/SiO_2). A solution of ammonium metatungstate hydrate ($(NH_4)_6H_2W_{12}O_{40}{\cdot}18H_2O$, 99.99 %, Sigma-Aldrich, Oakville, ON, Canada) was used to impregnate SiO_2 to produce a W/SiO_2 catalyst precursor with a target tungsten loading of 17 wt% (in W/SiO_2).

2.1.2 WP/SiO_2 Catalyst

Ammonium hydrogen phosphate ($(NH_4)_2HPO_4$, 99.99 %, Sigma-Aldrich, Oakville, ON, Canada) was dissolved in deionized water and mixed with a solution of ammonium metatungstate hydrate. The mixed solution was then used to impregnate SiO_2 to produce a WP/SiO_2 catalyst precursor. The amount of W precursor and P precursor were chosen to obtain 17 wt% W with a 1:1 molar ratio of W to P in the final WP/SiO_2 catalyst.

2.1.3 NiWP/SiO_2 Catalysts

For the NiWP/SiO_2 catalysts, the WP–impregnated silica samples were prepared first. These samples were dried at 393 K for 10 h, and then impregnated with aqueous solutions of nickel nitrate hexahydrate to obtain molar ratios of Ni to W of 0.4–1.0. The Ni-promoted SiO_2-supported WP catalysts were named according to the molar ratio of Ni, W, and P. For example, W/SiO_2 refers to a catalyst containing W, while NiWP/SiO_2 (0.6:1:1.6) refers to a catalyst containing Ni, W, and P in a molar ratio of 0.6:1:1.6 (Ni:W:P).

For comparison, all catalysts were treated under the same thermal conditions. The slurry containing the SiO_2 support and solution of precursors was put on a heating plate and stirred until visually dry. The catalyst sample was further dried at 393 K for 10 h and then heated at 5 K min^{-1} to 773 K and calcined in air for 6 h. The sample was reduced in flowing hydrogen (Praxair, 99.999 %, 100 mL min^{-1}) as the temperature was increased from room temperature to 1,023 K at a heating rate of 2 K min^{-1}, and then held at 1,023 K for 2 h. After cooling to room temperature in flowing H_2, the sample was purged with helium (Praxair, 99.999 %, 60 mL min^{-1}) for 10 min and then passivated by flowing 4.98 vol% oxygen (balance helium) at 60 mL min^{-1} over the sample for 30 min.

2.2 Catalyst Characterization

X-ray diffraction (XRD) powder patterns of the catalysts after calcination in air as well after reduction and passivation were obtained on a Multiflex X-ray diffractometer (Rigaku, Woodlands, TX, USA) using Cu K_α radiation ($\lambda = 1.54056$ Å), a 40 kV tube voltage, 20 mA tube current, and a scan rate of 2° min^{-1}. Crystallite sizes were calculated from the full width at half maximum of the XRD peak using the Scherrer equation; $D_c = K\lambda/(\beta\cos(\theta))$, where K is a constant taken as 0.9, λ is the wavelength of the X-ray radiation, β is the peak width in radians at half-maximum, and 2θ is the Bragg angle of the reflection.

Surface area and pore volume were measured by nitrogen physisorption at 77 K with a TriStar adsorption instrument (Micromeritics, Norcross, GA, USA). All reduced and passivated samples were degassed under vacuum (70 mTorr) at 523 K for 4 h prior to physisorption.

Carbon monoxide chemisorption was performed on a ChemBET-3000 adsorption instrument (Quantachrome, Boynton Beach, FL, USA) at 313 K. Prior to the analysis the reduced and passivated samples were re-reduced at 823 K for 2 h and then purged with helium at this temperature for 2 h before being cooled to the analysis temperature.

2.3 Activity Measurements

The experiments for pyridine HDN were performed in a high-pressure test rig. Hydrogen (Praxair, 99.999 %) was fed to the reactor via a calibrated mass flow controller while pyridine (C_5H_5N, ≥99 %, Sigma-Aldrich, Oakville, ON, Canada) was fed using a syringe pump into heated (453 K) lines to vaporize the liquid. The gaseous feeds

were mixed and introduced into the stainless steel tubular flow reactor that contained the catalyst. The product gas was depressurized and a slip stream was analyzed online by a GC–MS system (Agilent, FID and quadrupole mass spectrometer, column HP-plot Q).

All the experiments were conducted with 0.2 g of catalyst at a reaction pressure of 17.2 bar, and temperatures between 573 and 633 K with a liquid pyridine flow of 0.005 mL min^{-1}. The H_2 flow rate was 400 mL_N min^{-1}, resulting in a molar ratio of H_2:pyridine in the feed of 287:1. Prior to the activity measurements, the passivated catalysts were re-reduced in situ with hydrogen at 633 K. The setup did not allow a higher reduction temperature as was used prior to the CO-chemisorption measurements. All catalysts were initially reduced at the same temperature (1,023 K) and reduction at 633 K should be sufficient to reduce the surface oxides [2]. Experiments were conducted in the absence of sulfur, to avoid the influence of components such as hydrogen sulfide and thiophene on the HDN reactions [23].

The conversion of pyridine (X_{PYR}), the product selectivity (S_i), and yield (Y_i) were defined according to Eqs. 1–3, respectively, where $\dot{n}_i$ is the molar flow rate (mol s^{-1}) of the given species i.

$$X_{PYR} = \frac{\dot{n}_{PYR,in} - \dot{n}_{PYR,out}}{\dot{n}_{PYR,in}} \times 100\% \quad (1)$$

$$S_i = \frac{\dot{n}_{i,out}}{\dot{n}_{PYR,in} - \dot{n}_{PYR,out}} \times 100\% \quad (2)$$

$$Y_i = \frac{\dot{n}_{i,out}}{\dot{n}_{PYR,in}} \times 100\% \quad (3)$$

The specific pyridine conversion (r_{PYR}) normalized by the amount of catalyst, and turnover frequency were calculated with Eqs. 4 and 5, respectively:

$$r_{PYR} = \frac{\dot{n}_{PYR,in} - \dot{n}_{PYR,out}}{m_{catalyst}} \quad (4)$$

$$TOF_{PYR} = \frac{\dot{n}_{PYR,in} - \dot{n}_{PYR,out}}{CO_{uptake} \cdot m_{catalyst}} \quad (5)$$

3 Results and Discussion

3.1 Catalyst Characterization

The WP catalysts were analyzed with XRD after calcination (773 K) and then after reduction (1,023 K) to follow the crystalline transformation of W and WP. Figures 1 and 2 show the XRD profiles of W/SiO_2 and WP/SiO_2 catalysts, respectively, as well as the reference pattern for W, W_3O, WO_3 and WP taken from the JCPDS database (now called the International Centre for Diffraction Data,

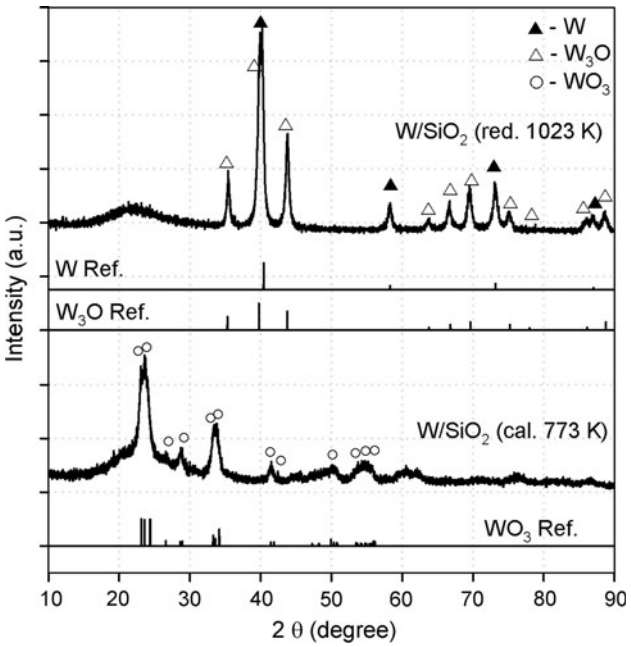

Fig. 1 XRD patterns of W/SiO_2 catalysts after calcination at 773 K (W/SiO_2 cal. 773 K) and reduction at 1,023 K (W/SiO_2 red. 1,023 K). References of W, W_3O, and WO_3 are from JCPDS 04-0806, JCPDS 41-1230, and JCPDS 43-1035, respectively

ICDD). In Fig. 1 W/SiO_2 calcined at 773 K had peaks corresponding to the crystallite structure of WO_3, which is fully oxidized tungsten oxide. After reduction at 1,023 K, peaks corresponding to the crystalline structures of W_3O and W were visible. The broad peak at $2\theta \approx 22°$ corresponds to the silica support. With the addition of phosphorous to W/SiO_2 (molar ratio W/P = 1), the tungsten species were amorphous after calcination at 773 K (Fig. 2, no peak for WO_3 was visible), but after reduction at 1,023 K, all peaks corresponded to WP and no peaks for W_3O were observed. Clark et al. [1] have reported similar results for unsupported WP catalysts. In contrast, Zuzaniuk and Prins [2] did not detect crystalline WP on a silica support until reduction at temperatures above 1,273 K. These authors used different reduction conditions (10 mL min^{-1} with 4.98 vol% hydrogen in argon) than the conditions used in this study (100 mL min^{-1} in pure hydrogen).

The XRD profiles of the Ni modified WP/SiO_2 catalysts are shown in Fig. 3 with the reference patterns for WP, W_3O and Ni_2P. Again, these catalysts were prepared by impregnation of a W + P solution followed by Ni addition with target molar ratios of Ni:W:P of 0.4:1:1.4, 0.6:1:1.6 and 1:1:2. In these catalysts, the total metal (Ni + W) to phosphorus ratio was 1:1. The XRD profile of the WP/SiO_2 catalyst had peaks corresponding only to WP. As the Ni content increased, the intensity of the peaks associated with WP decreased and peaks corresponding to W_3O appeared.

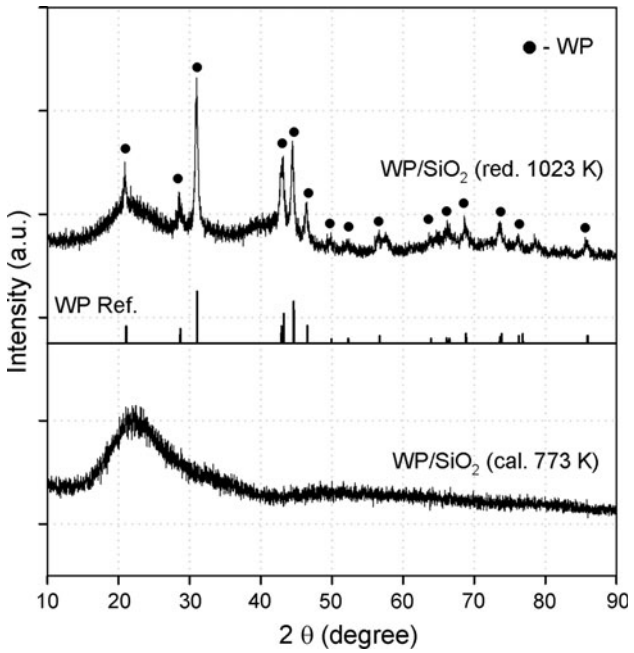

Fig. 2 XRD patterns of WP/SiO_2 catalyst after calcination at 773 K (WP/SiO_2 cal. 773 K) and reduction at 1,023 K (WP/SiO_2 red. 1,023 K). Reference of WP is from JCPDS 29-1364

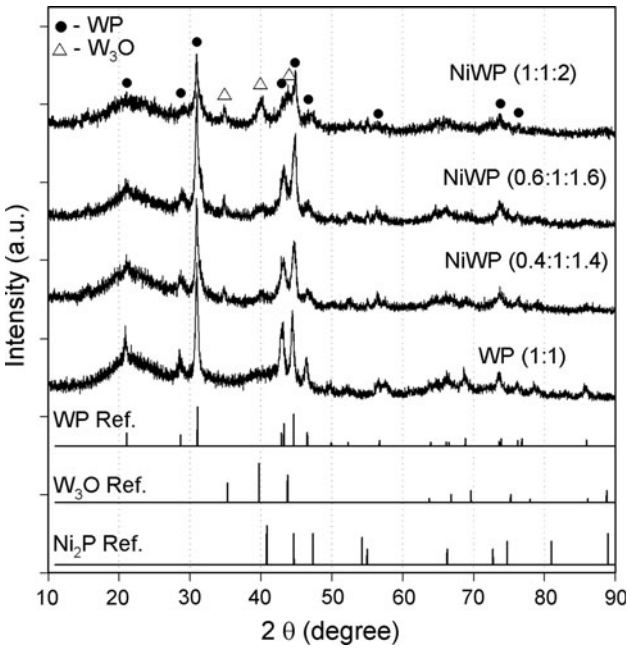

Fig. 3 XRD patterns of Ni added WP/SiO_2 catalysts with various molar ratios of Ni of 0.0–1.0. All catalysts were previously reduced at 1,023 K. References of WP, W_3O and Ni_2P are from JCPDS 29-1364, JCPDS 41 1230 and JCPDS 03-0953, respectively

No peaks corresponding to Ni such as NiO, NiP, Ni_2P, NiP_2, $Ni_{12}P_5$, $Ni(PO_3)_2$, NiP_4O_{11}, $Ni_2P_2O_7$, $Ni(NO_3)_2$, NiW, Ni_4W, $Ni_{17}W_3$, $NiWP_8$ or NiW_2P_3 were observed. Thus, Ni was present in an amorphous phase or in crystals too small to be detected by XRD. Zhao et al. [19] also could not identify the NiWP phase on a NiWP/AC catalyst and found that the main phase was WP as well.

The presence of W_3O in the $NiWP/SiO_2$ catalyst (1:1:2) was most likely due to the W–P dissociation caused by the stronger affinity of P for Ni than W. To further illustrate the competition between Ni and W for P, a catalyst with a Ni:W:P molar ratio of 1:1:1 (i.e., a total metal to P molar ratio of 2:1) was prepared and analyzed by XRD (Fig. 4, in this figure the XRD profile of the NiWP (1:1:2) is repeated from Fig. 3 for better comparison). With a reduced amount of phosphorus, Ni_2P and W crystallites were formed in addition to WP and W_3O. Izhar and Nagi [24] also observed WP, Ni_2P and W_3O crystallites in an unsupported NiWP system with a Ni:W molar ratio equal to one.

The XRD profiles of Ni/SiO_2 after calcination at 773 K and reduction at 1,023 K are illustrated in Fig. 5 with the reference patterns for NiO and Ni. As expected, peaks corresponding to NiO are present in the profile of the calcined catalyst while peaks corresponding to Ni are present in the profile of the reduced catalyst. Peaks associated with crystalline Ni were not visible on the NiWP catalysts after calcination (results not shown) or after

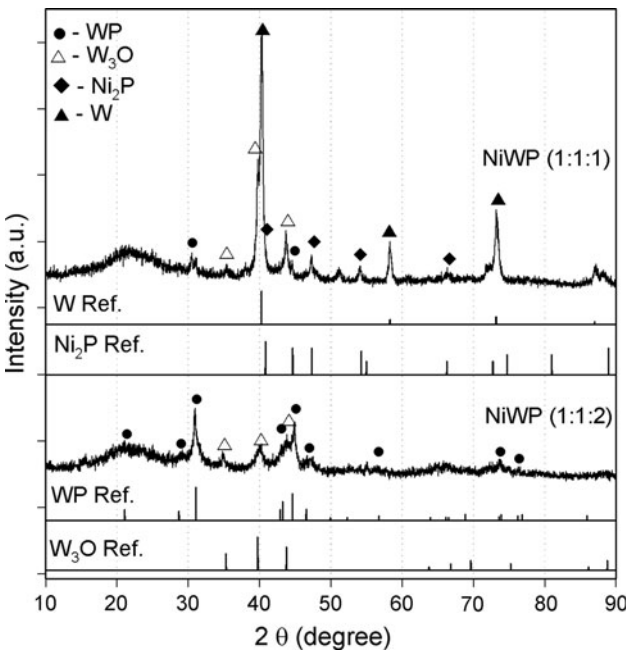

Fig. 4 XRD patterns of $NiWP/SiO_2$ (1:1:1) and $NiWP/SiO_2$ (1:1:2). All catalysts were previously reduced at 1,023 K. References of W, WP, W_3O and Ni_2P are from JCPDS 04-0806, JCPDS 29-1364, JCPDS 41-1230 and JCPDS 03-0953, respectively

reduction (Figs. 3, 4). As the silica was impregnated with W and P first and then with Ni, the presence of W and P evidently helped to disperse the Ni.

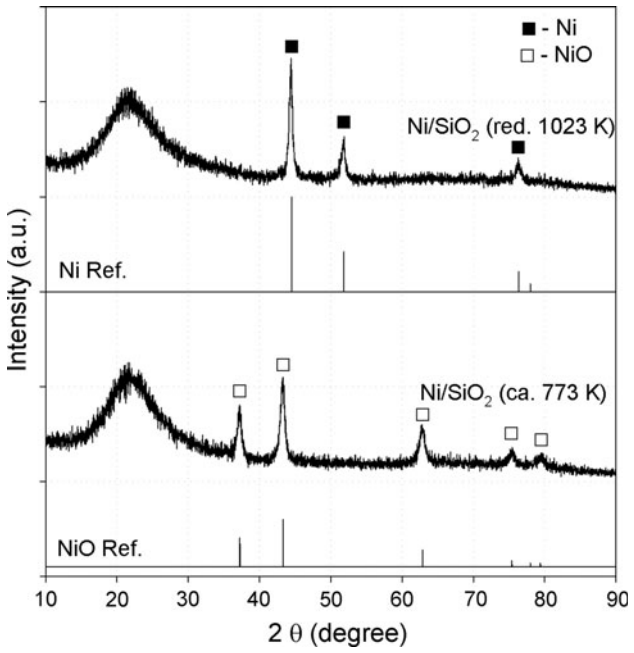

Fig. 5 XRD patterns of Ni/SiO_2 catalyst after calcination at 773 K (Ni/SiO_2 cal. 773 K) and reduction at 1,023 K (Ni/SiO_2 red. 1,023 K). References of Ni and NiO are from JCPDS 04-0850 and JCPDS 47-1049, respectively

The surface area (A_{BET}), pore volume (V_{Pore}), crystallite size (D_C) and crystallite identification of the catalysts investigated are summarized in Table 1. The silica support had a surface area of $\sim$285 $m^2\ g^{-1}$ and a pore volume of 1.12 mL g^{-1}, while the surface areas and pore volumes of the catalysts varied between 195 and 232 $m^2\ g^{-1}$, and 0.73–0.97 mL g^{-1}. The surface areas and pore volumes of catalysts are typically less than those of the support because impregnation and deposition of metals can result in blocked pores.

Crystallite diameters were estimated from the XRD profiles using the Scherrer equation and ranged between 14 and 24 nm. The W/SiO_2 and $NiWP/SiO_2$ (1:1:1) contained mainly W crystallites with diameters of 19 and 24 nm, respectively. The addition of Ni reduced the diameter of the WP crystallites from 20 to 15 nm. A further increase of the Ni content up to Ni:W:P ratio of 1:1:2 did not change the WP crystallite size significantly.

The XRD results, specifically the absence of peaks corresponding to Ni in the NiWP catalysts, suggested that the Ni was better dispersed when added to WP/SiO_2 than to SiO_2. The measured CO uptakes were consistent with this theory (Table 2). The CO uptake was significantly higher on the $NiWP/SiO_2$ catalysts (14–43 μmol g^{-1}) than on the Ni/SiO_2 catalyst (3.8 μmol g^{-1}). The increased CO uptake for $NiWP/SiO_2$ catalysts is mainly attributed to the addition of Ni sites, but also to the higher dispersion and smaller WP crystallite sizes.

3.2 Activity Measurements

The pyridine hydrodenitrogenation was conducted at temperatures of 573–633 K, a total pressure of 17.2 bar, a hydrogen gas flow rate of 400 $mL_N\ min^{-1}$, and a pyridine liquid flow rate of 0.005 mL min^{-1}. The following catalysts were tested: WP/SiO_2, $NiWP/SiO_2$ (0.4:1:1.4), $NiWP/SiO_2$ (0.6:1:1.6), and $NiWP/SiO_2$ (1:1:2).

The results for the pyridine conversion and then the results for the product yield and selectivity are discussed to evaluate the investigated catalysts. The conversion of pyridine as a function of the reaction temperature is illustrated in Fig. 6. The lowest conversion was obtained with the WP/SiO_2 catalyst. Here the conversion values increased from 5.3 to 8.9 % for 573–633 K, respectively. Adding Ni to the WP/SiO_2 catalyst increased the hydrogenation of pyridine consistent with the higher CO uptakes on the Ni promoted catalysts (Table 2). The conversion of pyridine over the $NiWP/SiO_2$ (1:1:2) catalyst was more than double that over the WP/SiO_2 catalyst for all investigated temperatures. The TOF_{PYR} values, however, decreased with increasing Ni content; for example the $NiWP/SiO_2$ (1:1:2)

Table 1 Physiochemical data for the investigated catalysts (reduced at 1,023 K)

Catalyst	Ni (wt%)	W (wt%)	P (wt%)	Ni:W:P molar ratio	A_{BET} ($m^2\ g^{-1}$)	V_{Pore} (mL g^{-1})	D_C (nm)	Crystallite observed by XRD
SiO_2	–	–	–	–	285	1.12	–	–
W/SiO_2	–	17	–	–	232	0.88	19 (W)	W, W_3O
WP/SiO_2	–	17	2.9	1:1	210	0.80	20 (WP)	WP
$NiWP/SiO_2$	2.2	17	4.0	0.4:1:1.4	212	0.82	15 (WP)	WP, W_3O
$NiWP/SiO_2$	3.3	17	4.6	0.6:1:1.6	195	0.73	16 (WP)	WP, W_3O
$NiWP/SiO_2$	5.4	17	5.7	1:1:2	196	0.74	14 (WP)	WP, W_3O
$NiWP/SiO_2$	5.4	17	2.9	1:1:1	202	0.81	24 (W), [a](WP)	W, Ni_2P, WP, W_3O
Ni/SiO_2	6.1	–	–	–	252	0.97	17 (Ni)	Ni

[a] The crystallite size for WP on this catalyst could not be determined because of the small XRD peak size (Fig. 4)

Table 2 CO chemisorption capacities and activities for the HDN of pyridine over silica supported WP and NiWP catalysts measured at 633 K and 17.2 bar

Catalyst	Ni:W:P	CO - uptake	Pyridine conversion			Selectivity			
	molar ratio	(μmol g^{-1})	X_{PYR} (mol%)	r_{PYR} (μmol $s^{-1}g^{-1}$)	TOF_{PYR} (× 10^3 s^{-1})	THP (mol%)	PIP (mol%)	PA (mol%)	PENT (mol%)
WP/SiO_2	1:1	6	8.9	0.458	76.5	3.9	57.3	7.0	23.9
$NiWP/SiO_2$	0.4:1:1.4	14	14.8	0.767	53.9	8.0	52.2	13.1	21.6
$NiWP/SiO_2$	0.6:1:1.6	21	18.1	0.934	45.0	6.2	45.6	16.8	26.2
$NiWP/SiO_2$	1:1:2	43	18.9	0.977	22.7	7.7	34.6	13.5	37.1

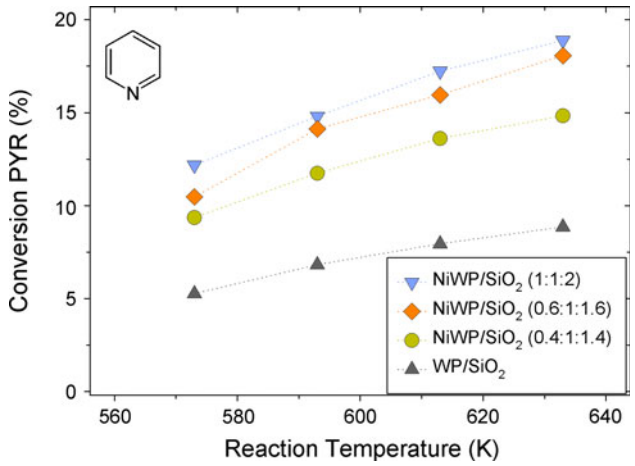

Fig. 6 Conversion of pyridine as a function of temperature (573–633 K) for WP/SiO_2, $NiWP/SiO_2$ (0.4:1:1.4), $NiWP/SiO_2$ (0.6:1:1.6), and $NiWP/SiO_2$ (1:1:2) catalysts

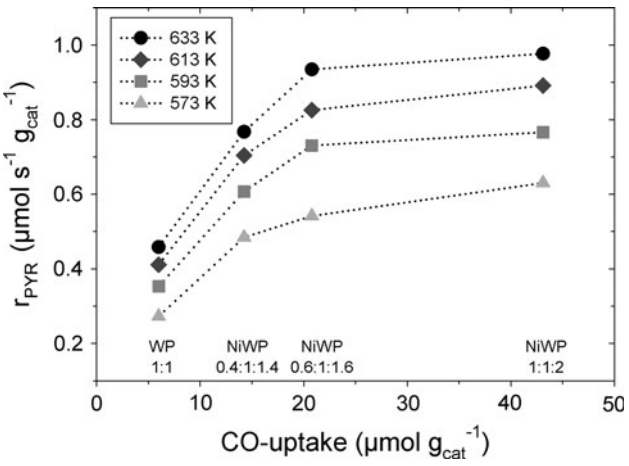

Fig. 7 Specific pyridine conversion at 573–633 K as a function of the CO-uptake for WP/SiO_2, $NiWP/SiO_2$ (0.4:1:1.4), $NiWP/SiO_2$ (0.6:1:1.6), and $NiWP/SiO_2$ (1:1:2) catalysts

catalyst had a ~70 % lower TOF_{PYR} value compared with the WP/SiO_2 catalyst as shown for 633 K in Table 2.

The CO-uptake of the $NiWP/SiO_2$ (1:1:2) catalyst was more than seven, three and two times higher than that of the WP/SiO_2 (1:1), $NiWP/SiO_2$ (0.4:1:1.4) and $NiWP/SiO_2$ (0.6:1:1.6) catalysts, respectively. The specific pyridine conversion rates, however, did not increase by the same factor. The increase was much smaller, as shown in Fig. 7, and in fact the specific pyridine conversion for the $NiWP/SiO_2$ (1:1:2) was only slightly higher than for the $NiWP/SiO_2$ (0.6:1:1.6). An explanation for this behavior might be the different adsorption mechanisms and/or sites for CO and pyridine adsorption on the investigated catalysts. CO was adsorbed at 313 K and did not react on the surface, whereas pyridine was adsorbed at reaction temperatures (i.e., 573–633 K), and reacted further with hydrogen and formed surface intermediates and products. The adsorbed species might inhibit further pyridine adsorption and conversion as shown in [25, 26]. The Arrhenius plot in Fig. 8 is consistent with product inhibition as the change in pyridine conversion rates is greater from 573 to 593 K than from 593 to 633 K. The observed activation energies for the pyridine hydrogenation of $E_{obs} = 24.5 \pm 2.0$ kJ mol^{-1} did not differ significantly for the four catalysts investigated. Pille and Fromment [26] estimated an activation energy of 57.8 kJ mol^{-1} on a $NiMoP/Al_2O_3$ catalyst and Anabtawi et al. [27] reported a value of 57.3 kJ mol^{-1} on a NiW/Al_2O_3 catalyst. The low observed activation energy in this study is likely a consequence of the heat of adsorption of pyridine being lumped with the rate constant, which leads to $E_{obs} = \Delta H_{PYR} + E_A$. The reaction was not diffusion controlled according to the Weisz-criteria (see supplementary information).

The main reaction products that were identified are pyridine (PYR, reactant), 2,3,4,5-tetrahydropyridine (THP, intermediate), piperidine (PIP, intermediate), pentylamine (PA, intermediate) and pentane (PENT, desired). At higher temperatures (i.e., 613 and 633 K) small amounts of cyclopentane, butane and *n*–pentylpiperidine were identified as well. The product distributions for (a) THP, (b) PIP, (c) PA and (d) PENT are illustrated in Figs. 9 and 10 as yields and selectivities, respectively. The THP yields were

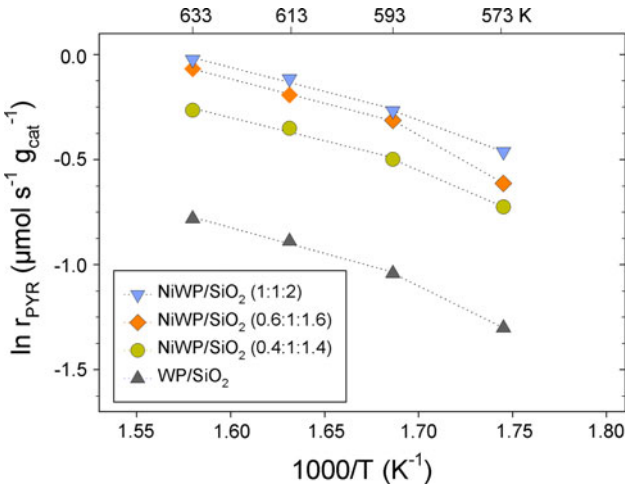

Fig. 8 Arrhenius plot for the pyridine hydrogenation at 573–633 K for WP/SiO_2, NiWP/SiO_2 (0.4:1:1.4), NiWP/SiO_2 (0.6:1:1.6), and NiWP/SiO_2 (1:1:2) catalysts

almost constant in the investigated temperature range, with NiWP/SiO_2 (1:1:2) having the highest and WP/SiO_2 the lowest yields of ~1.3 and ~0.3 %, respectively. The PIP yields for all four catalysts increased, went through a maximum and decreased with increasing temperature. With increasing Ni content the maximum in the PIP yield shifted towards lower temperatures and decreased more quickly. For the NiWP/SiO_2 (1:1:2) catalyst the PIP yield decreased from 10.5 to 6.5 % for 593–633 K, which indicates that at higher temperatures PIP is converted to PA and PENT as shown in Fig. 9c, d. Here the PENT yield reached values of 7 % for the NiWP/SiO_2 (1:1:2) and only 2.1 % for the WP/SiO_2 catalyst at 633 K. Thus, adding nickel to the WP/SiO_2 not only enhanced the hydrogenation of PYR, but also favored the conversion of PIP to PA and PENT. The NiWP/SiO_2 (1:1:2) catalyst had the lowest selectivity to PIP (34.6 % at 633 K) and highest selectivity to PENT (37 % at 633 K) compared with the other catalysts (Fig. 10 and Table 2).

The yields and selectivities for PA increased with temperature and did not decline as expected for an intermediate as observed for THP and PIP. This result might suggest that the desorbed PA in the gas phase does not re-adsorb again, because the surface is covered with PYR, PIP and NH_3, all of which adsorb strongly [28–30]. Under the present experimental conditions the surface intermediate PA either desorbs from the catalyst surface or reacts to PENT and NH_3. To verify the proposed mechanism for our investigated transition metal phosphide catalysts, spectroscopic methods such as in situ DRIFTS measurements are required. In addition, kinetic studies including model discrimination will help to identify the most likely reaction mechanism based on extended experiments and modeling.

These results indicate that promoting tungsten phosphide with nickel enhanced the hydrogenation activity and resulted in higher selectivity to saturated hydrocarbons such as pentane. Adding Ni to WP had a similar effect for the HDN of pyridine as was observed for the HDN of carbazole over NiMoP catalysts [13]. Specifically, the Ni-

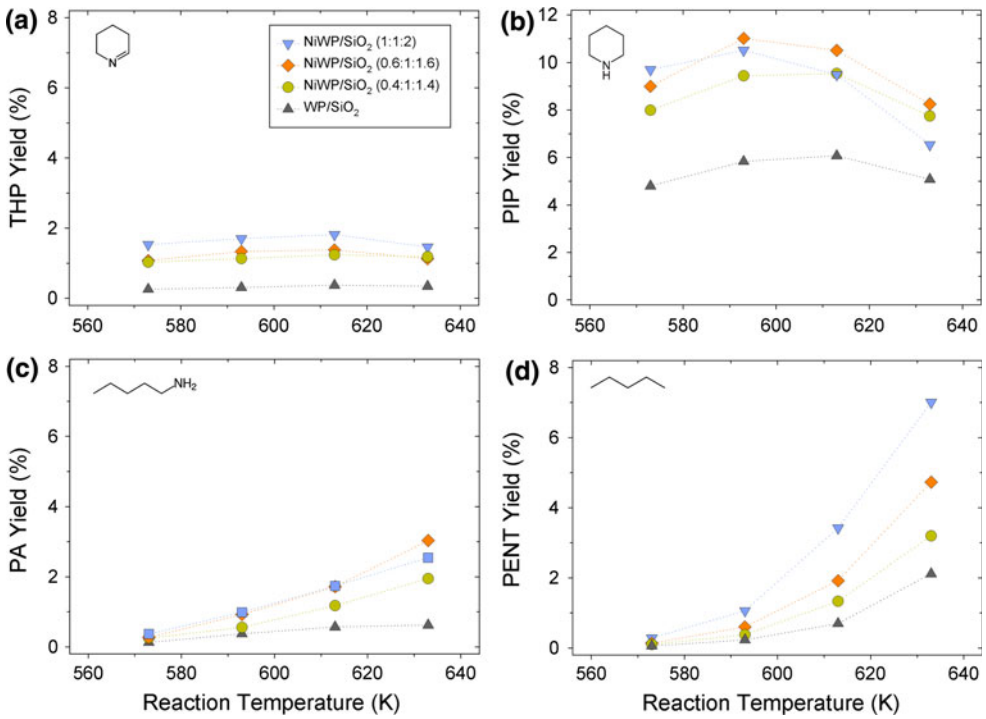

Fig. 9 Product yield of the HDN of pyridine as a function of temperature (573–633 K) for WP/SiO_2, NiWP/SiO_2 (0.4:1:1.4), NiWP/SiO_2 (0.6:1:1.6), and NiWP/SiO_2 (1:1:2) catalysts

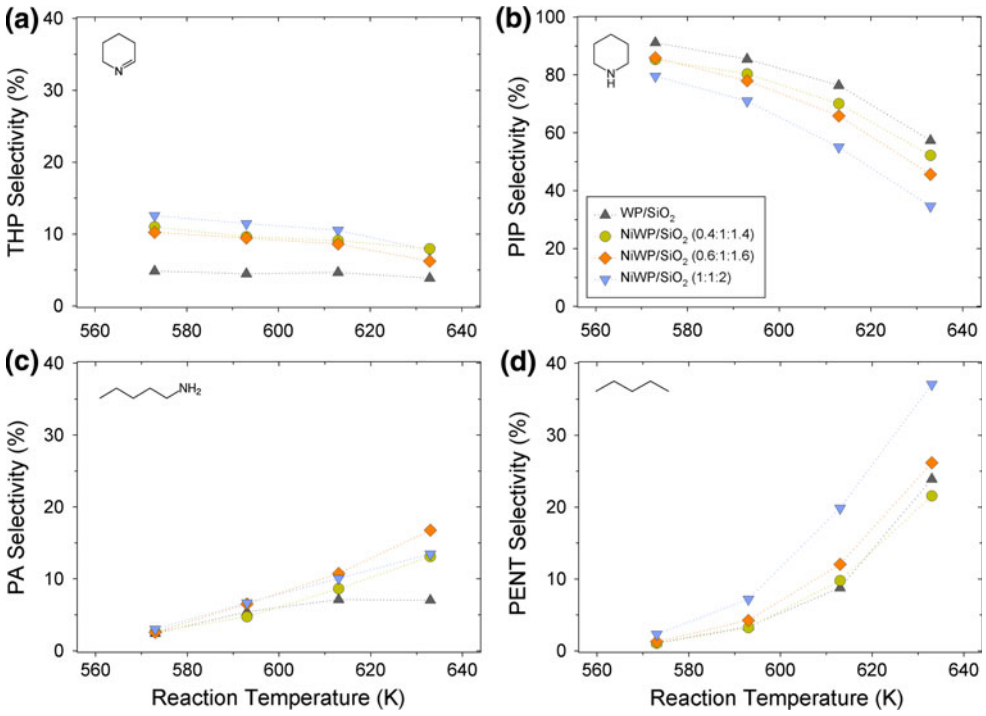

Fig. 10 Product selectivities of the HDN of pyridine as a function of temperature (573–633 K) for WP/SiO_2, $NiWP/SiO_2$ (0.4:1:1.4), $NiWP/SiO_2$ (0.6:1:1.6), and $NiWP/SiO_2$ (1:1:2) catalysts

promoted metal phosphide catalyst had lower TOF values compared with the un-promoted catalyst but the selectivity to the desired product pentane was increased by adding nickel due to enhanced hydrogenation and C–N bond cleavage.

4 Conclusions

In this work, the HDN of pyridine over $NiWP/SiO_2$ catalysts was studied. These catalysts were prepared such that Ni_2P crystalline did not form even though Ni competed with W to combine with P. The Ni species were not observed as crystallites on the WP/SiO_2 catalysts, but did cause the dissociation of W–P bonds and resulted in W_3O crystallites in addition to the WP crystallites on the catalysts.

The NiWP catalysts had a lower TOF value for the HDN of pyridine compared with the WP catalyst but were more selective to the desired product of pentane. On a mass basis, the nickel containing WP catalysts had higher HDN activity—the NiWP (1:1:2) catalyst was twice as active as the WP catalyst. The better pentane selectivity of the NiWP catalysts can be explained by the enhanced hydrogenation and increased C–N bond breakage.

Acknowledgments Funding from Suncor Energy Inc. for this project is gratefully acknowledged. The authors would also like to thank Elsa Ramirez for assisting with the activity measurements.

References

1. Clark P, Li W, Oyama ST (2001) J Catal 200:140
2. Zuzaniuk V, Prins R (2003) J Catal 219:85
3. Shu Y, Oyama ST (2005) Carbon 43:1517
4. Ibeh B, Zhang S, Hill JM (2009) Appl Catal A 368:127
5. Sun F, Wu W, Wu Z, Guo J, Wei Z, Yang Y, Jiang Z, Tian F, Li C (2004) J Catal 228:298
6. Lee YK, Oyama ST (2006) J Catal 239:376
7. Cecilia J, Infantes-Molina A, Rodriguez-Castellon E, Jimenez-Lopez A (2009) J Catal 263:4
8. Da Silva VT, Sousa L, Amorim R, Andrini L, Figueroa S, Requejo F, Vicentini FC (2011) J Catal 279:88
9. Duan X, Li X, Wang A, Teng Y, Wang Y, Hu Y (2010) Catal Today 149:11
10. Teng Y, Wang A, Li X, Xie J, Wang Y, Hu Y (2009) J Catal 266:369
11. Hayes JR, Bowker RH, Gaudette AF, Smith MC, Moak CE, Nam CY, Pratum TK, Bussell ME (2010) J Catal 276:249
12. Abu II, Smith KJ (2007) Appl Catal A 328:58
13. Abu II, Smith KJ (2007) Catal Today 125:248
14. Abu II, Smith KJ (2006) J Catal 241:356
15. Burns AW, Gaudette AF, Bussell ME (2008) J Catal 260:262
16. Ding L, Shu Y, Wang A, Zheng M, Li L, Wang X, Zhang T (2010) Appl Catal A 385:232
17. Gaudette AF, Burns AW, Hayes JR, Smith MC, Seda T, Bussell ME (2010) J Catal 272:18
18. Oyama ST, Zhao H, Freund H-J, Asakura K, Wlodarczyk R, Sierka M (2012) J Catal 285:1
19. Zhao G, Zheng M, Wang A, Zhang T (2010) Chin J Catal 31:928
20. Oyama ST (2003) J Catal 216:343
21. Sawhill SJ, Phillips DC, Bussell ME (2003) J Catal 215:208
22. Sawhill SJ, Layman KA, Van Wyk DR, Engelhard MH, Wang C, Bussell ME (2005) J Catal 231:300
23. Furimsky E, Massoth FE (2005) Catal Rev Sci Eng 47:297

24. Izhar S, Nagai M (2009) Catal Today 146:172
25. McIlvried HG (1971) Ind Eng Chem Process Des Dev 10:125
26. Pille R, Froment G (1997) Stud Surf Sci Catal 106:403
27. Anabtawi JA, Mann RS, Khulbe KC (1980) J Catal 63:456
28. Hanlon RT (1987) Energy Fuels 1:424
29. Machida M, Sakao Y, Ono S (2000) Appl Catal A 201:115
30. Sonnemans J, Van Den Berg GH, Mars P (1973) J Catal 31:220